ARTICLE

ACS chemical biology

Structure-Based Design of a Periplasmic Binding Protein Antagonist that Prevents Domain Closure

M. Jack Borrok, Yimin Zhu[‡], Katrina T. Forest[§,*], and Laura L. Kiessling[,‡,*]

Departments of [†]Biochemistry, [‡]Chemistry, and [§]Bacteriology, University of Wisconsin, Madison, Wisconsin 53706

ABSTRACT Many receptors undergo ligand-induced conformational changes to initiate signal transduction. Periplasmic binding proteins (PBPs) are bacterial receptors that exhibit dramatic conformational changes upon ligand binding. These proteins mediate a wide variety of fundamental processes including transport, chemotaxis, and quorum sensing. Despite the importance of these receptors, no PBP antagonists have been identified and characterized. In this study, we identify 3-*O*-methyl-D-glucose as an antagonist of glucose/galactose-binding protein and demonstrate that it inhibits glucose chemotaxis in *E. coli*. Using small-angle X-ray scattering and X-ray crystallography, we show that this antagonist acts as a wedge. It prevents the large-scale domain closure that gives rise to the active signaling state. Guided by these results and the structures of open and closed glucose/galactose-binding protein, we designed and synthesized an antagonist composed of two linked glucose residues. These findings provide a blueprint for the design of new bacterial PBP inhibitors. Given the key role of PBPs in microbial physiology, we anticipate that PBP antagonists will have widespread uses as probes and antimicrobial agents.

Periplasmic binding proteins (PBPs) are nonenzymatic receptors used by bacteria to sense small molecules and transport them into the cytoplasm. Most PBPs participate in the transport of solute molecules into the cytoplasm *via* ABC transporters (*1*). Their targets include critical nutrients such as carbohydrates, amino acids, vitamins, and ions. PBPs also function in chemotaxis, quorum sensing, and other signaling systems (*2*–*4*). Members of the large and diverse PBP family are ubiquitous in both Gram-negative and Gram-positive bacteria (Gram-positive PBPs are membrane-bound lipoproteins). The general "Venus-flytrap" architecture of PBPs, consisting of two globular domains connected by a small hinge region, is also found in intracellular bacterial proteins (such as the lac repressor) and eukaryotic receptors (such as glutamate and GABA receptors) (*1, 5*).

PBPs exist in open and closed forms in solution, and in the absence of ligand, the open form predominates (*6, 7*). Open PBPs adopt a range of conformations as evidenced by multiple distinct open structures of ribose-binding protein, allose-binding protein, leucine/isoleucine/valine-binding protein, and leucine-binding protein (*8*–*12*). The binding of a ligand elicits a dramatic conformational change, such that the ligand is clamped between the two lobes. The resulting complex possesses a protein-binding surface not present in the open form; therefore, the complex can be recognized by membrane-bound receptors (*13*). Thus, ligand binding acts as a switch to toggle PBPs between inactive open forms and active closed forms.

Because of their prevalence in bacteria and involvement in processes vital for pathogenesis and metabolism, PBPs can serve as potential targets of antimicrobial agents. For example, in some pathogenic bacteria,

*Corresponding authors,
forest@bact.wisc.edu,
kiessling@chem.wisc.edu.

Received for review January 28, 2009
and accepted April 4, 2009.

Published online April 6, 2009

10.1021/cb900021q CCC: $40.75

signaling *via* PBPs can facilitate virulence (*14–19*). Indeed, certain sideromycin antibiotics, such as albomycin, act through PBPs. Mimicking natural siderophores, these antibiotics can gain access to the cell interior by binding to a PBP; once inside, they kill the cell (*20*). Like all known physiological PBP ligands, these antibiotics bind and stabilize the closed form, and thereby act as PBP agonists. Though compounds that interfere with conformational change in a eukaryotic PBP-like receptor have been described (*21*), no PBP antagonists that bind and stabilize the inactive form have been identified. Compounds that prevent the conformational change leading to the closed signaling state could disrupt fundamental physiological processes such as chemotaxis, transport, or quorum sensing.

Herein, we describe a PBP antagonist and a structure-based design strategy to devise new antagonists. Specifically, we found that 3-*O*-methyl-D-glucose (3-OMe Glc) blocks the function of the *Escherichia coli* PBP glucose/galactose-binding protein (GGBP). GGBP mediates the uptake of the sugars D-glucose, D-galactose, and their derivatives (*22*). It also facilitates chemotaxis by signaling through the Trg chemoreceptor (*23*), and this response provides a means to identify antagonists. The binding of 3-OMe Glc to GGBP not only fails to elicit chemotaxis but also blocks chemotactic responses to glucose. Three-dimensional structural studies reveal that the ability of 3-OMe Glc to inhibit chemotaxis arises because its binding precludes GGBP closure. Using our understanding of the molecular basis for 3-OMe Glc inhibition, we applied structure-based design to generate a dimeric antagonist that is more potent than 3-OMe Glc. Because PBP domain closure is critical for function, the use of dimeric compounds to wedge open PBPs serves as a general strategy for antagonist design.

RESULTS

3-OMe Glc Is a GGBP Antagonist. Glucose derivatives have been shown previously to bind to GGBP and induce signaling (*24–27*). For example, polymers possessing glucose and galactose residues linked *via* the anomeric position are potent chemoattractants that bind GGBP, whereas sugars with alkoxy substituents at the 3-position are not (*28*). Although the GGBP binding site exhibits considerable plasticity (*25, 28*), the simplest explanation for this lack of activity is that 3-position sugar derivatives do not bind GGBP. We sought to test this assumption and assessed the binding of 3-OMe Glc for GGBP using a ^{14}C galactose competition assay (*29*). These experiments reveal that 3-OMe Glc competes with ^{14}C galactose (Supplementary Figure S1). Whereas the K_i for glucose is 0.5 $\pm$ 0.04 μM, 3-OMe Glc has a K_i of 125 $\pm$ 15 μM. Thus, though its affinity is weaker than that of glucose or galactose, 3-OMe Glc is a GGBP ligand.

Given the unexpected ability of 3-OMe Glc to bind to GGBP, we asked whether this ligand could promote chemotaxis. Motile bacteria seek out attractants and avoid repellents by toggling between two modes of locomotion: running and tumbling. Attractants, such as glucose or ribose, promote an increase in the "running" or straight-swimming bias of cells, whereas the addition of repellents (or a decrease in attractant concentration) causes an increase in the frequency of "tumbling" or disorganized flagellar motion. Attractant or repellent responses to ligands can be quantified by analyzing the average angular velocity of a bacterial population upon addition of chemoeffector (*30, 31*). A decrease in the average angular velocity of a population of motile cells corresponds with an attractant (running) response, whereas an increase in average angular velocity corresponds with a repellent (tumbling) response. We used motion analysis to measure the average angular velocity of *E. coli* in the presence of 3-OMe Glc. The results indicate that this glucose analogue is neither an attractant nor a repellent. Even at a concentration 40-fold greater than its K_i (Figure 1, panel a), it fails to elicit a chemotactic response. In light of these data, we tested whether 3-OMe Glc can inhibit glucose chemotaxis. The diminishing response of *E. coli* to glucose in the presence of increasing concentrations of 3-OMe Glc indicates that 3-OMe Glc blocks chemotactic responses to glucose (Figure 1, panel a).

The inhibitory activity of 3-OMe Glc may stem from its ability to sequester GGBP in a state that precludes interaction with Trg. Alternatively, 3-OMe Glc may generate the ternary complex with GGBP and Trg, but the complex may have impaired signaling capabilities. To distinguish between these possibilities, we exploited observations that ribose-binding protein (RBP) also facilitates chemotaxis through an interaction with Trg (*32*). If 3-OMe Glc promotes the formation of inactive ternary complex containing Trg, chemotactic responses to ribose should be impaired. We therefore measured the response of *E. coli* to ribose in the presence of 3-OMe Glc. The 3-substituted sugar derivative did not impede

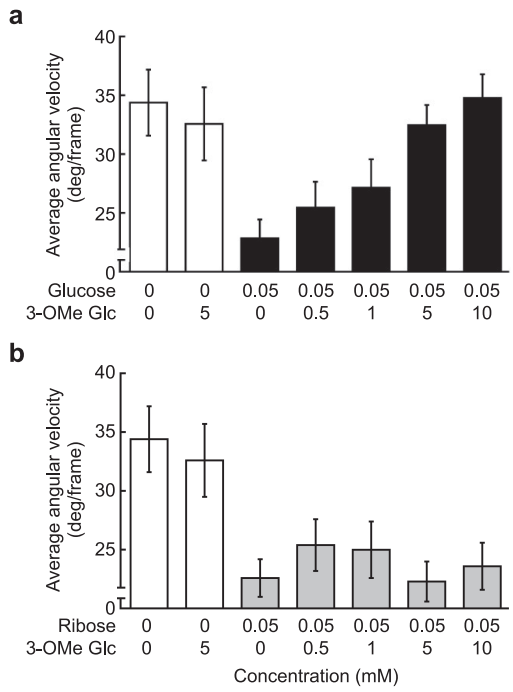

Figure 1. Compound 3-OMe Glc inhibits chemotaxis toward glucose but not ribose. Motion analysis of wild-type *E. coli* (AW607) upon treatment with glucose (panel a) or ribose (panel b) in the presence of increasing concentrations of 3-OMe Glc was performed on at least three independent experiments of 6−8 s duration. Videos were recorded within 45 s of stimulant addition. Error bars are given in 2σ uncertainties.

the attractant response to ribose (Figure 1, panel b). The finding that RBP-Trg signaling is unaffected by 3-OMe Glc indicates that the complex between GGBP and 3-OMe Glc does not effectively bind to Trg.

3-OMe Glc-Bound GGBP Is Open in Solution. Our binding and chemotaxis data suggest that 3-OMe Glc stabilizes an open state of GGBP. To test this hypothesis directly, small-angle X-ray scattering (SAXS) was employed. SAXS allows for accurate and precise measurement of a protein's radius of gyration (R_g), and the method has been used previously to differentiate between open and closed states of periplasmic binding proteins, including GGBP (*7, 33*). Upon PBP closure in solution, a characteristic 1.5−2 Å decrease in R_g occurs. R_g values for unbound, glucose-bound, and 3-OMe Glc-bound GGBP in solution were obtained from experimental scattering data using the Guinier approximation:

$$\ln I(Q) = \ln I(0) - R_g^2 Q^2/3$$

In this approximation, the scattering vector $Q = 4\pi \sin\theta/\lambda$ (λ, wavelength; 2θ, scattering angle), and $I(Q)$ is the scattering intensity at Q. R_g is calculated from the slope of a Guinier plot ($\ln I(Q)$ *vs* Q^2) in the $QR_g < 1$ region (*34, 35*). The R_g values of 22.7 ± 0.1 Å for unbound GGBP and 21.1 ± 0.1 Å for glucose-bound GGBP (Figure 2, panel a) are in agreement with published SAXS measurements (*7*) and values calculated from structures determined by X-ray crystallography (Supplementary Table 1). The complex of 3-OMe Glc and GGBP had an R_g value of 22.4 ± 0.1, indicating that 3-OMe Glc binds to an open form of GGBP.

Structure of the Complex between 3-*O*-Me Glc and GGBP Provides a Mechanism for Antagonism. We sought to better understand the molecular interactions that allow 3-OMe Glc to bind to GGBP and yet maintain the open form. Inspection of a closed, glucose-bound GGBP structure (*36*) suggests that the addition of a methyl group at the 3-OH position could disrupt hydrogen bonding interactions and cause steric clashes with Asn211 and Asp236. This structure analysis predicts that, in the absence of significant rearrangement, the 3-methyl substituent will prevent 3-OMe Glc from binding in the same orientation as glucose or galactose. To assess the validity of this model, we solved a 3-OMe Glc-bound GGBP structure using X-ray crystallography.

Using our previously identified crystallization conditions (*36*), we grew large crystals of GGBP in the absence of ligand; 3-OMe Glc was then added to crystallization drops such that its final concentration was 5 mM. Data to 1.7 Å resolution were collected, and the structure was solved by molecular replacement with open unbound GGBP (PDB ID: 2FW0) as the starting model (Table 1). In contrast, when unbound GGBP crystals were soaked with glucose, diffraction was completely abolished, presumably because glucose promotes closure of GGBP and thereby destroys the lattice packing. The addition of 3-OMe Glc did result in a change in the *b* and *c* unit cell dimensions by +6% and −2%, respectively (Table 1), but it caused no deterioration in diffraction quality.

Unbound GGBP crystallizes in the open state with a citrate−sodium complex in the sugar binding cleft (*36*). No electron density resembling this complex was obtained from 3-OMe Glc-soaked crystals. In difference density maps, a large feature above Trp183 was ob-

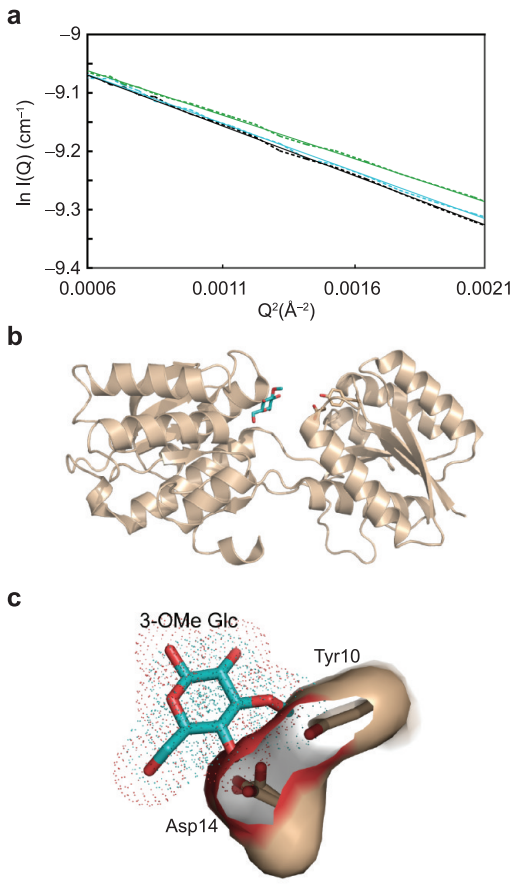

Figure 2. Complex of 3-OMe Glc and GGBP is in an open conformation. a) SAXS data (dotted lines) from unliganded GGBP (black), 3-OMe Glc-bound GGBP (cyan), or glucose-bound GGBP (green). Linear fits of these data (solid lines) in the $0.021 > Q > 0.046$ region were used to determine slope and R_g. b) 3-OMe Glc (cyan sticks) binds to the C-terminal domain of the open conformation of GGBP (brown ribbons). Side chains of Tyr10 and Asp14 (shown as brown sticks) would undergo steric clashes upon closure. c) Superposition of the C-terminal domain of the 3-OMe Glc-bound complex onto the C-terminal domain of the glucose-bound structure. The depiction highlights steric clashes with side chains (cyan sticks with calculated molecular surface) that prevent formation of the closed signaling state of GGBP when 3-OMe Glc binds.

served. After refinement of protein side chains and water molecules, several orientations of 3-OMe Glc were fit to determine which best matched this density (Supplementary Figure S2). The results indicate that 3-OMe binds in a different orientation than glucose (*vide infra*). As a consequence, the GGBP complex retains an open conformation like that of the unbound protein (Figure 2, panel b). The complex differs from the unbound, open conformation by only a 4° hinge motion. This result supports the assertion that the crystalline structure is a valid model of the open solution conformation observed in SAXS experiments (Supplementary Table 1). The final refined structure is of high quality with good geometry (Table 1).

The structure of the 3-OMe Glc−GGBP complex provides insight into why the ligand prevents closure of GGBP. Superposition of the C-terminal domain of the 3-OMe Glc-bound GGBP structure onto the C-terminal domain of the glucose-bound GGBP structure reveals

TABLE 1. Data collection and refinement statistics

Data collection	
Space group	$P2_12_12_1$
Cell dimensions	
a, *b*, *c* (Å)[a]	56.9, 74.7, 110.1
Resolution (Å)[b]	55−1.7 (1.75−1.7)
R_{sym}	3.4 (25.9)
I/σ_I	26.6 (5.8)
Completeness (%)	90.1 (56.8)
Redundancy	6.3 (2.1)
Refinement	
Resolution (Å)[b]	40−1.7 (1.74−1.7)
No. reflections	43,596 (1886)
R_{work}/R_{free}	18.2/20.4 (24.4/25.9)
No. atoms	
Protein	2361
Water	351
Ligand/ions	16
B-factors	
Protein	12.0
Water	22.6
Ligand/ions	38.0
Rms deviations	
Bond lengths (Å)	0.012
Bond angles (deg)	1.30
PDB code	2QW1

[a]For comparison, before soaking *a*, *b*, and $c = 56.8$, 70.3, and 112.1 Å, respectively. [b]Values in parentheses are for the highest-resolution shell.

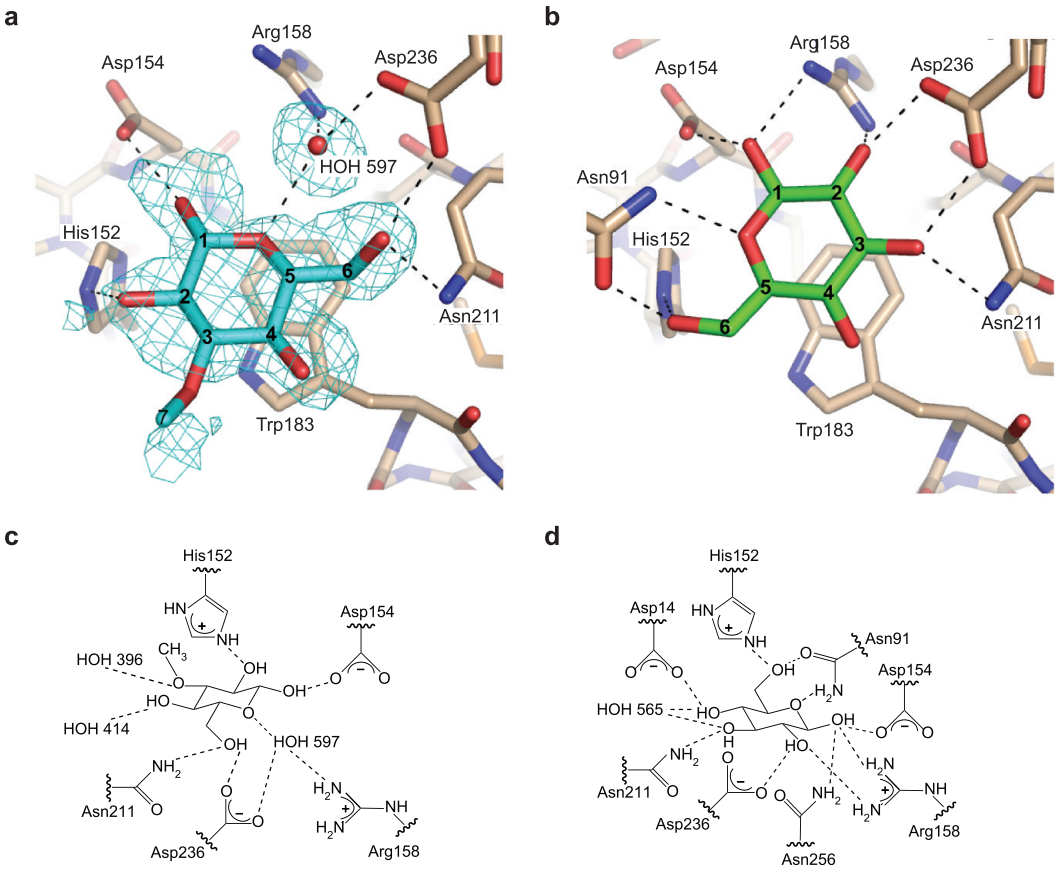

Figure 3. Structure of 3-OMe Glc bound to GGBP determined by X-ray crystallography. a) An F_o-F_c map (cyan mesh, contoured at 2.5σ) was generated with 3-OMe Glc (cyan) and HOH 597 omitted. b) Glucose (green) bound to GGBP (PDB ID: 2FVY) is depicted, along with putative hydrogen bonds to selected residues in the C terminal domain cleft. Complete hydrogen bonding networks for 3-OMe Glc (panel c) and glucose (panel d) are illustrated.

that upon domain closure, the sugar derivative would engage in unfavorable steric interactions with residues in the N-terminal region of the binding cleft. Specifically, the methoxy group of the ligand would clash with the aromatic ring of Tyr10 and the 4-hydroxyl group of the ligand with the carboxylate side chain of Asp14 (Figure 2, panel c). Thus, GGBP cannot bind 3-OMe Glc and achieve a closed state required for productive interaction with Trg.

Binding Orientation of 3-OMe Glc Differs from That of Glucose. A comparison of the GGBP complexes of glucose and 3-OMe Glc reveals differences in the orientations of these sugar ligands. Although glucose makes contacts with both GGBP domains, 3-OMe Glc is situated in the C-terminal side of the sugar binding cleft of open GGBP. Though in their complexes both sugars stack on Trp183, 3-OMe Glc is flipped, rotated, and translated when compared to the bound glucose (Figure 3, panels a and b). Despite this reorientation, 3-OMe Glc interacts with many of the same residues as glucose (Figure 3, panels c and d). Specifically, Asn211, Asp236, Asp154, and His152 all participate in hydrogen bonds in both ligand bound complexes. Moreover, in both structures, the anomeric position of the bound sugar is exclusively in the β configuration (*36*). In the 3-OMe Glc structure a water molecule (H_2O 597) occupies the position of the sugar O2 atom in the glucose-bound structure. This water molecule can engage in hydrogen bonding with Asp236, Arg158 and the O5 position of 3-OMe Glc (Figure 3, panel a). The O3 and

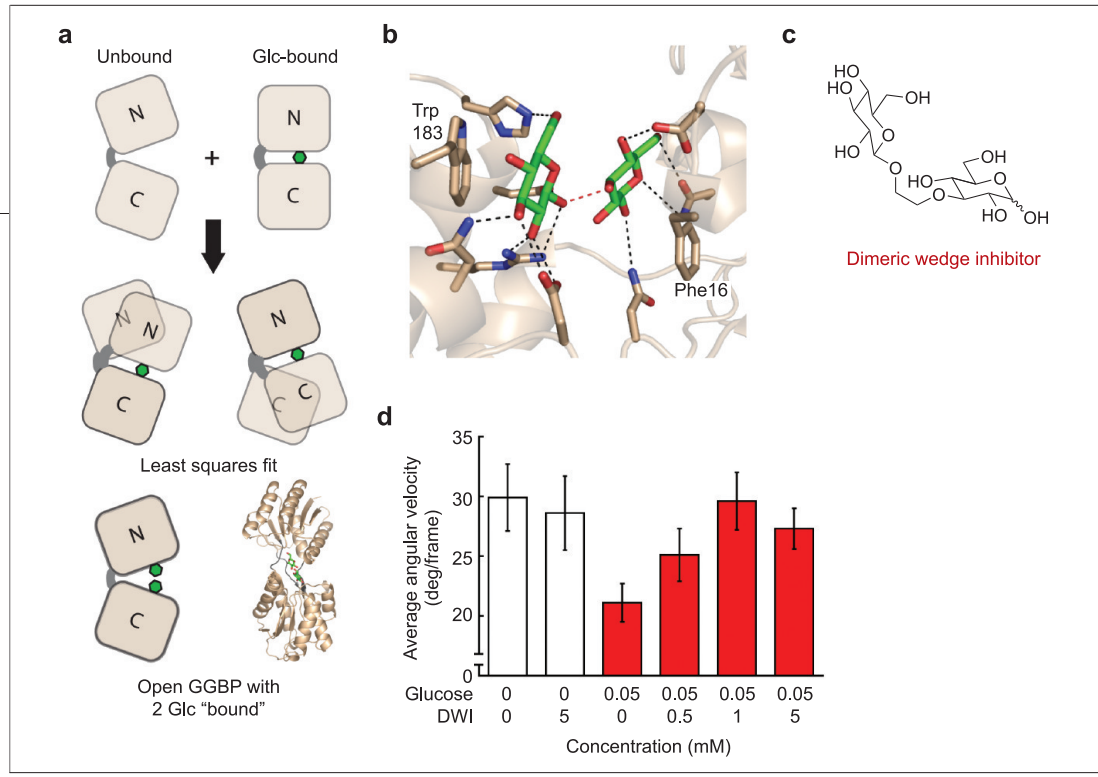

Figure 4. Design strategy for an inhibitor that stabilizes the open form of GGBP. a) Structures of closed, glucose-bound GGBP (PDB ID: 2FVY) and open, unliganded GGBP (PDB ID: 2FW0) were used to generate an unbound model with one glucose molecule occupying each side of the binding cleft. b) In this model, many stacking and hydrogen bonding interactions in the closed form are maintained (black dashes). c) Two glucose molecules can be covalently linked at the 1 and 3 positions with an ethylene tether to form the dimeric wedge inhibitor (DWI, 3-*O*-(2′-β-D-glucopyranosyloxyethyl)-D-glucose). d) Chemotactic responses to glucose in *E. coli* (AW607) cells were inhibited by the DWI. Motion analysis error bars are given in 2σ uncertainties.

O4 substituents of 3-OMe Glc, which protrude into the open binding cleft, do not interact with side chains.

Structure-Based Design of a Dimeric PBP Inhibitor. Our finding that 3-OMe Glc acts as a GGBP antagonist by preventing closure prompted us to devise a general strategy for designing periplasmic binding protein inhibitors. Specifically, we considered how to design a compound that could satisfy key hydrogen bonding and hydrophobic stacking interactions present in the closed, glucose-bound form and yet serve as a wedge. To this end, we created a model of open GGBP with a glucose molecule bound in either side of the binding cleft. Using least-squares superpositioning, we overlaid either the N- or the C- terminal domain of the closed structure onto the open structure (Figure 4, panel a). These models suggested that the cleft of GGBP could accommodate the two resulting glucose molecules (Figure 4, panel b). Moreover, it appeared to be chemically feasible to link these two glucose molecules, thereby creating a dimeric wedge inhibitor (DWI, 3-*O*-(2′-β-D-glucopyranosyloxyethyl)-D-glucose) that would allow each glucose moiety to form numerous contacts with either the N- or the C-terminal residues in the binding site. Specifically, we envisioned connecting the 1 position of a glucose residue to the 3 position of another. We used a 2-methylene linker to tether the two residues because it could position the two sugars in an orientation similar to that in the model (Figure 4, panel c).

Binding and Chemotaxis Experiments with the DWI. We used chemical synthesis to produce the putative antagonist DWI. Briefly, an ethylene glycol unit was appended to the 3-position of a protected glucose derivative, and the resulting compound was used in a glycosylation reaction with a protected glucosyl donor. Protecting group removal afforded the DWI. The ability of this diglucose derivative to bind to GGBP was tested using the aforementioned ^{14}C galactose competition assay. Intriguingly, the dimeric compound bound with higher affinity ($K_i = 27 \pm 7$ μM) than does 3-OMe Glc (Supplementary Figure S1).

Given the ability of the DWI to bind GGBP, we next tested its ability to act as an antagonist of chemotaxis. If this compound can indeed function as a wedge, it should promote the open, nonproductive form of GGBP. Alternatively, the dimer might bind in the canonical mode (*i.e.*, to the closed form) and promote chemotaxis. Motion analysis experiments (Figure 4, panel d) indicate that the DWI inhibits glucose chemotaxis. These results validate our structure-based design strategy.

DISCUSSION

The widespread distribution and fundamental roles of bacterial PBPs suggest that members of this protein family are targets for antimicrobial agents. Moreover, antagonists of PBPs can serve as useful probes. To realize these applications however, PBP antagonists must be identified. The physiological PBP ligands identified to date shift the equilibrium from the open to the closed forms of the proteins. This observation led to a paradigmatic model for PBP function; domain closure upon ligand binding creates a binding interface for the PBP to interact with a transmembrane receptor to signal its occupancy state. This model is supported by the observation that an engineered interdomain disulfide bond within maltose-binding protein results in a covalently locked closed form that signals in the *absence* of ligand (*37*). Our results provide complementary evidence for this model; we show in two cases that binding of a ligand that prevents domain closure blocks PBP signaling. Specifically, we used SAXS and X-ray crystallographic analysis to demonstrate that the 3-OMe Glc-bound GGBP exists in an open state. Consistent with our structural data, we found that 3-OMe Glc is an inhibitor of glucose chemotaxis in *E. coli*. By identifying a nonsignaling, ligand-bound state of GGBP, our data indicate that ligands can be used to lock native PBPs in unbound nonfunctional states.

In retrospect, the ability of 3-OMe Glc to hold GGBP in an open form likely arises from the unique properties of glucose and its derivatives. In the thermodynamically preferred pyranose form, all of the substituents are equatorial, which results in a radial display of groups. This structural attribute is consistent with our findings that 3-OMe Glc and glucose both can bind to GGBP but do so in different orientations. What would not have been predicted from this analysis, however, is that complexation of 3-OMe Glc would stabilize the open form of GGBP. This observation provided impetus to search for other antagonists that would bind and stabilize the open form of the PBP.

In principle, high-throughput screening methods can be used to identify small molecule PBP antagonists. Indeed, a high-throughput virtual screening targeted at LuxP (a PBP involved in quorum sensing) has recently yielded inhibitors of *Vibrio harveyi* bioluminescence (*38*); however, the mechanism of inhibition of these compounds remains unknown. We postulated that the wealth of information on PBP structure and function might yield a generalizable, rational approach. Guided by the structure of GGBP in the open (unbound) and closed (bound) GGBP conformations, we conceived a general design strategy: create a dimeric ligand that can interact simultaneously with both the N- and C-terminal domains and yet prevent domain closure. To test this hypothesis, we synthesized the dimeric glucose derivative DWI and demonstrated that it possesses the expected antagonistic activity and also has higher affinity for GGBP than does 3-OMe Glc. Because PBPs share a common architecture and hinge motion upon opening and closing, we anticipate that our approach can serve as a roadmap for designing antagonists for a wide variety of PBPs important in pathogenesis (*2, 14–19*). By overlaying the N- and C-terminal domains of the closed forms (*2, 18*) of two quorum sensing PBPs (LsrB and LuxP) with their respective open forms (*18, 39*), we generated models of the open forms with two autoinducer-2 (AI-2) molecules bound (Figure 5). These models could serve as starting points for the rational design of PBP inhibitors that satisfy hydrogen bonding and hydrophobic interactions of the two ligands and yet prevent domain closure. Moreover, we envision that using combinatorial chemistry along with our structure-based design strategy can expedite the generation of highly potent PBP antagonists.

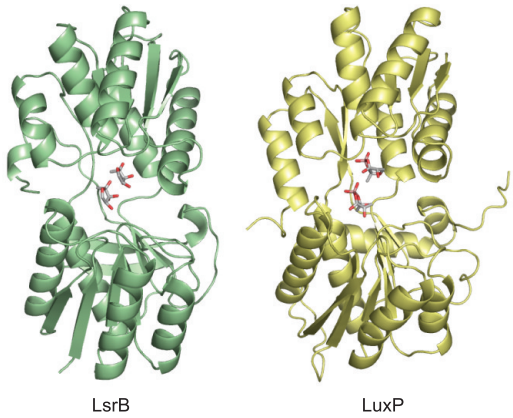

Figure 5. Structures of other PBPs indicate that our antagonist design strategy is broadly applicable. Open, unbound and closed, ligand-bound structures of the quorum sensing PBPs LsrB (green, PDB codes 1TJY and 1TM2) and LuxP (yellow, PDB codes 1JX6 and 1ZHH) were used to generate open models with two AI-2 molecules bound to each cleft.

METHODS

Protein Expression and Purification. GGBP was purified from *E. coli* strain HB929 harboring the pVB2 plasmid (kindly provided by G. Hazelbauer, U. Missouri-Columbia) using a method similar to that reported previously (*25*). Cells were grown to an OD_{600} of ~0.6 in tryptone broth supplemented with 0.2% glucose and 100 μg mL^{-1} ampicillin. Cells were centrifuged and transferred into tryptone broth containing 100 μg mL^{-1} ampicillin and no glucose and grown for 4 h. Cells were then harvested, and periplasmic content was collected using the osmotic shock method (*22*). GGBP was further purified with a Q-Sepharose Fast Flow column (Amersham) in a 0−0.25 M NaCl gradient in 10 mM Tris-HCl buffer (pH 8.3). GGBP eluted as the salt concentration of the eluent approached ~0.1 M. Purified protein was exhaustively dialyzed against 2 M guanidine-HCl, 25 mM Tris-HCl, pH 8.0 and 1 mM EDTA. Folded GGBP was obtained by further dialysis into buffer containing 10 mM Tris-HCl, pH 7.3 and 1 mM $CaCl_2$. Protein concentration was determined using the bicinchoninic acid (BCA) method.

^{14}C Galactose Competition Binding Assays. The ^{14}C galactose competition assay was carried out using a procedure similar to that described previously (*29*). GGBP (2 mg mL^{-1} final concentration) was incubated for 15 min at 25 °C with ^{14}C galactose (Sigma; final concentration of 25 μM) and various concentrations of competing ligand or buffer in a 1.5 mL tube (20 μL total volume). This solution was then placed on a square of nitrocellulose paper, which was submerged in saturated ammonium sulfate solution repeatedly to precipitate ligand-bound protein and remove excess ^{14}C galactose. The nitrocellulose paper with precipitated protein was placed in a scintillation vial, 10 mL scintillation fluid was added, and radioactivity was measured. K_i values were calculated from the experimentally determined IC_{50} values using the Cheng−Prusoff equation (*40*).

Motion Analysis Video Microscopy. The method of preparation of *E. coli* for motion analysis was similar to that described previously (*26*). Chemotactic wild-type *E. coli* (AW607) cells were taken from the outer edge of a 0.3% agar LB swim plate and grown in LB broth (supplemented with 0.1% glucose and 0.1% ribose) to an OD_{600} of 0.3. Cells were washed twice in chemotaxis buffer (10 mM potassium phosphate buffer, pH 7.0 and 10 μM ethylene diamine tetraacetic acid). Bacteria were then diluted with chemotaxis buffer to an OD_{600} of approximately 0.1. Cells were suspended in this buffer approximately 30 min before the motion analysis experiments were conducted to promote expression of GGBP and RBP. Motile *E. coli* cells (4 μL) were then placed under a coverslip supported by additional coverslips and allowed to adapt for 2−3 min. Stimulant or buffer (1 μL) was added, and bacterial movement within the first 45 s was recorded (*30, 31*). Bacterial paths were plotted using DataPoint, v0.62 (Glenn A. Carlson; Xannah Applied Science and Engineering), and mean angular velocities were calculated and averaged using Microsoft Excel.

SAXS Data Collection and Analysis. Prior to the SAXS experiments, purified unbound GGBP was further dialyzed into a 10 mM Tris-HCl (pH 7.2), 1 mM $CaCl_2$ solution containing 50 mM ethylene glycol as a cryoprotectant. The dialysis buffer was preserved for background measurements. Ligand (glucose at 0.5 mM or 3-OMe Glc at 5 mM) or buffer was added and GGBP (1 mg mL^{-1}) was centrifuged at 12,000 rpm for 5 min to remove any precipitated material prior to data collection. SAXS data were collected at BioCAT, Beamline 18ID of the Advanced Photon Source (Argonne, IL) (*41*) with a CCD camera (Aviex). The sample temperature was approximately 15 °C. The sample to detector distance was 2428 mm with X-rays at 12 KeV. The protein solution was pumped continuously through a 1 mm quartz capillary cell to minimize radiation damage. Approximately thirty 1.5 s exposures of the empty cell, buffer alone (with the ligand being tested), or GGBP with ligand in buffer were collected. Averaging of frames, corrections for detector response and beam intensity, mask exclusion, and buffer subtraction were carried out using IGOR Pro (Wavemetrics) and the BioCAT macros written by Liang Guo (BioCAT). The radius of gyration (R_g), which is defined as the rms distance of all atoms from their common center of mass, was derived using the Guinier approximation in regions where $QR_g < 1$. The program CRYSOL (*42*) was used to derive R_g values from the unliganded GGBP structure (PDB ID: 2FW0), glucose-bound GGBP (PDB ID: 2FVY), and 3-OMe Glc-bound GGBP.

X-ray Crystallography. Unliganded crystals were obtained in hanging drops using equal volumes of 25 mg mL^{-1} GGBP and a mother liquor of 2.0 M ammonium sulfate and 0.05 M sodium citrate dihydrate, as described (*36*). To a large crystal within a 3 μL hanging drop, 2 μL of a 5 mM 3-OMe Glc containing mother liquor was added. After ~15 min, 2 μL was removed and replaced with 2 μL of fresh 3-OMe Glc containing mother liquor; this procedure was repeated 4 times. Cryocooling was achieved by swiping the crystal in a cryoprotectant solution containing sodium malonate (2.0 M) and 3-*O*-methyl glucose (5 mM) before immersion in liquid nitrogen.

A diffraction data set from the 3-OMe Glc-soaked crystal was collected on a Proteum CCD detector with X-rays generated by a Microstar rotating anode (Bruker AXS). Images were processed with Proteum software (Bruker AXS). Phases were determined by molecular replacement using Amore with the unliganded GGBP (PDB ID: 2FW0) structure as a starting model. The structure was initially refined using CNS (*43*). Refmac (*44*) was used for later rounds of refinement (the R_{free} reflection set was maintained). Manual fitting between refinement rounds was performed in XFIT (*45*). No electron density was detected for residues 1 or 307−309; these residues were left out of the final model. After multiple rounds of refinement, the 3-OMe Glc ligand was fit into planar F_o–F_c density above Trp183 in several orientations. The best and final 3-OMe Glc orientation yielded negligible difference density upon refinement (Supplementary Figure S2). No attempt was made to fit a mixture of orientations due to the relatively limited resolution of these data, but we do not discount the possibility that other orientations may be present in a small fraction of the 3-OMe Glc-bound GGBP molecules. Figures were generated with Pymol (*46*).

Synthesis of the Dimeric Wedge Inhibitor. 1,2,4,6-Tetra-*O*-acetyl-3-*O*-allyl-β-D-glucopyranose was synthesized following the literature procedure (*47*). A solution of this sugar derivative (3.94 g, 10.1 mmol) in methylene chloride (35 mL) was cooled at −78 °C and sparged with ozone. After 30 min, the mixture was quenched with dimethyl sulfide (1.5 mL, 20.4 mmol). The mixture was stirred at RT overnight and concentrated *in vacuo*. The residue was dissolved in ethanol (25 mL). To the solution at 0 °C was slowly added sodium borohydride (0.38 g, 10 mmol). The mixture was stirred at 0 °C for 2 h, and excess sodium borohydride was quenched with dilute hydrochloric acid. The reaction mixture was diluted with methylene chloride and washed with water and brine, respectively. The organic solution was dried over magnesium sulfate, concentrated, and purified by column chromatography (1:2 hexane−EtOAc, then EtOAc) to give 3-*O*-(2′-hydroxyethyl)-1,2,4,6-*O*-tetraacetyl-glucose (3.03 g) in 76% yield. ^{1}H NMR: δ 5.66 (1H, d), 5.09 (2H, m), 4.25 (1H, dd), 4.09 (1H, dd), 3.78 (1H, m), 3.67 (3H, m), 3.62 (2H, M), 2.48 (OH, b), 2.11 (s, 6H), 2.10 (s, 3H), 2.08 (s, 3H). ^{13}C NMR: δ 170.74, 169.77, 169.54, 169.22, 91.83, 80.90, 74.25, 72.81, 71.53, 69.09, 61.76, 61.64, 20.83, 20.85, 20.76, 20.72. HRMS: calcd for $[M + Na]^+$ *m/e* 415.1216; found *m/e* 415.1204.

A mixture of 3-*O*-(2′-hydroxyethyl)-1,2,4,6-*O*-tetraacetyl-glucose (0.78 g, 2 mmol), 2,3,4,6-*O*-tetraacetylglucopyranosyl trichloroacetimidate (1.3 g, 2.7 mmol), and molecular sieves

(1.5 g) in methylene chloride (30 mL) was stirred at RT for 30 min. The mixture was then cooled to 0 °C, and trimethylsilyl triflate (0.04 mL, 0.2 mmol) was added. The mixture was warmed to RT overnight. The reaction was quenched by addition of aqueous sodium bicarbonate solution. The molecular sieves were removed by filtration and washed with methylene chloride. The combined organic solution was washed with brine and concentrated. The product was purified by column chromatography (1:2 hexanes−EtOAc, then EtOAc) to give the protected dimer as a light brown solid (0.875 g, 61%). ^{1}H NMR: δ 5.65 (1H, d), 5.21 (1H, t), 5.10 (3H, m), 4.96 (1H, dd), 4.56 (1H, d), 4.42 (1H, dd), 4.25 (1H, dd), 4.11 (1H, dd), 4.09 (1H, dd), 3.84 (1H, m), 3.76−3.65 (5H, m), 3.61 (1H, m), 2.11 (3H, s), 2.10 (6H, s), 2.09 (3H, s), 2.08 (3H, s), 2.06 (3H, s), 2.03 (3H, s), 2.00 (3H, s). ^{13}C NMR: δ 170.65, 170.58, 170.18, 169.43, 169.26, 169.16, 169.13, 100.45, 91.86, 80.36, 72.86, 72.84, 71.79, 71.27, 71.19, 70.70, 68.82, 68.68, 68.32, 61.86, 61.79, 20.84, 20.71, 20.68, 20.58. HRMS: calcd for $[M + Na]^+$ *m*/*e* 745.2167; found *m*/*e* 745.2182.

To a solution of the protected dimer (0.74 g, 1.03 mmol) in methanol (10 mL) was added sodium hydride (60% in mineral oil, 8 mg, 0.2 mmol) at 0 °C, and the mixture was stirred at RT for 6 h. The reaction was quenched by addition of Amberlite IR120 H^+ resin. The solution was diluted with water and washed with methylene chloride. The solvent was removed *in vacuo*, and the product, 3-*O*-(2′-β-D-glucopyranosyloxyethyl)-D-glucose, was purified by column chromatography (60:39:1 methylene chloride−methanol−water, then 50:40:10 methylene chloride−methanol−water) to give the desired dimer as a light brown solid (0.378 g, 95%). ^{1}H NMR: δ 5.11 (H1-α, d), 4.61 (H1-β, d), 4.41 (H1′-β, d), 4.12−3.17 (mH, m) ^{13}C NMR: δ 102.15, 95.73, 92.00, 84.82, 82.15, 75.90. 75.69, 75.62, 73.59, 73.08, 71.62, 71.46, 71.39, 71.02, 70.85, 70.62, 69.56, 69.40, 69.34, 69.18, 69.12, 62.78, 60.69, 60.58, 60.41, 48.96, 48.65. HRMS: calcd for $[M + Na]^+$ *m*/*e* 409.1322; found *m*/*e* 409.1316.

Acknowledgment: Research funding was provided by the National Institutes of Health (GM059984, L.L.K.) and the W. M. Keck Foundation (K.T.F.). M.J.B. was supported by a NIH Molecular Biosciences Training Grant (GM07215).

Supporting Information Available: This material is available free of charge *via* the Internet at http://pubs.acs.org.

REFERENCES

1. Tam, R., and Saier, M. H. (1993) Structural, functional, and evolutionary relationships among extracellular solute-binding receptors of bacteria, *Microbiol. Rev. 57*, 320–346.
2. Chen, X., Schauder, S., Potier, N., Van Dorsselaer, A., Pelczer, I., Bassler, B. L., and Hughson, F. M. (2002) Structural identification of a bacterial quorum-sensing signal containing boron, *Nature (London) 415*, 545–549.
3. Quiocho, F. A., and Ledvina, P. S. (1996) Atomic structure and specificity of bacterial periplasmic receptors for active transport and chemotaxis: variation of common themes, *Mol. Microbiol. 20*, 17–25.
4. Surin, B. P., Rosenberg, H., and Cox, G. B. (1985) Phosphate specific transport system of *Escherichia coli* nucleotide sequence and gene polypeptide relationships, *J. Bacteriol. 161*, 189–198.
5. Felder, C. B., Graul, R. C., Lee, A. Y., Merkle, H. P., and Sadee, W. (1999) The Venus flytrap of periplasmic binding proteins: an ancient protein module present in multiple drug receptors, *AAPS PharmSci. 1*, E2.
6. Carrithers, M. D., and Lerner, M. R. (1996) Synthesis and characterization of bivalent peptide ligands targeted to G-protein-coupled receptors, *Chem. Biol. 3*, 537–542.
7. Shilton, B. H., Flocco, M. M., Nilsson, M., and Mowbray, S. L. (1996) Conformational changes of three periplasmic receptors for bacterial chemotaxis and transport: the maltose-, glucose/galactose- and ribose-binding proteins, *J. Mol. Biol. 264*, 350–363.
8. Bjorkman, A. J., and Mowbray, S. L. (1998) Multiple open forms of ribose-binding protein trace the path of its conformational change, *J. Mol. Biol. 279*, 651–664.
9. Magnusson, U., Chaudhuri, B. N., Ko, J., Park, C., Jones, T. A., and Mowbray, S. L. (2002) Hinge-bending motion of D-allose-binding protein from *Escherichia coli*: three open conformations, *J. Biol. Chem. 277*, 14077–14084.
10. Magnusson, U., Salopek-Sondi, B., Luck, L. A., and Mowbray, S. L. (2004) X-ray structures of the leucine-binding protein illustrate conformational changes and the basis of ligand specificity, *J. Biol. Chem. 279*, 8747–8752.
11. Sack, J. S., Trakhanov, S. D., Tsigannik, I. H., and Quiocho, F. A. (1989) Structure of the L-leucine-binding protein refined at 2.4 Å resolution and comparison with the Leu/Ile/Val-binding protein structure, *J. Mol. Biol. 206*, 193–207.
12. Trakhanov, S., Vyas, N. K., Luecke, H., Kristensen, D. M., Ma, J., and Quiocho, F. A. (2005) Ligand-free and -bound structures of the binding protein (LivJ) of the *Escherichia coli* ABC leucine/isoleucine/valine transport system: trajectory and dynamics of the interdomain rotation and ligand specificity, *Biochemistry 44*, 6597–6608.
13. Hollenstein, K., Frei, D. C., and Locher, K. P. (2007) Structure of an ABC transporter in complex with its binding protein, *Nature (London) 446*, 213–216.
14. Eakanunkul, S., Lukat-Rodgers, G. S., Sumithran, S., Ghosh, A., Rodgers, K. R., Dawson, J. H., and Wilks, A. (2005) Characterization of the periplasmic heme-binding protein ShuT from the heme uptake system of *Shigella dysenteriae*, *Biochemistry 44*, 13179–13191.
15. Jin, B., Newton, S. M. C., Shao, Y., Jiang, X., Charbit, A., and Klebba, P. E. (2006) Iron acquisition systems for ferric hydroxamates, haemin and haemoglobin in *Listeria monocytogenes*, *Mol. Microbiol. 59*, 1185–1198.
16. Kemner, J. M., Liang, X. Y., and Nester, E. W. (1997) The *Agrobacterium tumefaciens* virulence gene chvE is part of a putative ABC-type sugar transport operon, *J. Bacteriol. 179*, 2452–2458.
17. Mason, K. M., Munson, R. S., and Bakaletz, L. O. (2005) A mutation in the sap operon attenuates survival of nontypeable *Haemophilus influenzae* in a chinchilla model of otitis media, *Infect. Immun. 73*, 599–608.
18. Miller, S. T., Xavier, K. B., Campagna, S. R., Taga, M. E., Semmelhack, M. F., Bassler, B. L., and Hughson, F. M. (2004) *Salmonella typhimurium* recognizes a chemically distinct form of the bacterial quorum-sensing signal AI-2, *Mol. Cell 15*, 677–687.
19. Parralopez, C., Baer, M. T., and Groisman, E. A. (1993) Molecular genetic analysis of a locus required for resistance to antimicrobial peptides in *Salmonella typhimurium*, *EMBO J. 12*, 4053–4062.
20. Clarke, T. E., Braun, V., Winkelmann, G., Tari, L. W., and Vogel, H. J. (2002) X-ray crystallographic structures of the *Escherichia coli* periplasmic protein FhuD bound to hydroxamate-type siderophores and the antibiotic albomycin, *J. Biol. Chem. 277*, 13966–13972.
21. Armstrong, N., and Gouaux, E. (2000) Mechanisms for activation and antagonism of an AMPA-sensitive glutamate receptor: Crystal structures of the GluR2 ligand binding core, *Neuron 28*, 165–181.
22. Anraku, Y. (1968) Transport of sugars and amino acids in bacteria. I. Purification and specificity of the galactose- and leucine-binding proteins, *J. Biol. Chem. 243*, 3116–3122.
23. Hazelbauer, G. L., and Adler, J. (1971) Role of galactose binding protein in chemotaxis of *Escherichia coli* toward galactose, *Nature-New Biol. 230*, 101–104.
24. Gestwicki, J. E., and Kiessling, L. L. (2002) Inter-receptor communication through arrays of bacterial chemoreceptors, *Nature (London) 415*, 81–84.

25. Gestwicki, J. E., Strong, L. E., Borchardt, S. L., Cairo, C. W., Schnoes, A. M., and Kiessling, L. L. (2001) Designed potent multivalent chemoattractants for *Escherichia coli*, *Bioorg. Med. Chem. 9*, 2387–2393.
26. Gestwicki, J. E., Strong, L. E., and Kiessling, L. L. (2000) Tuning chemotactic responses with synthetic multivalent ligands, *Chem. Biol. 7*, 583–591.
27. Lamanna, A. C., Gestwicki, J. E., Strong, L. E., Borchardt, S. L., Owen, R. M., and Kiessling, L. L. (2002) Conserved amplification of chemotactic responses through chemoreceptor interactions, *J. Bacteriol. 184*, 4981–4987.
28. Adler, J., Hazelbauer, G. L., and Dahl, M. M. (1973) Chemotaxis toward sugars in *Escherichia coli*, *J. Bacteriol. 115*, 824–847.
29. Zukin, R. S., Strange, P. G., Heavey, L. R., and Koshland, D. E. (1977) Properties of Galactose Binding-Protein of *Salmonella typhimurium* and *Escherichia coli*, *Biochemistry 16*, 381–386.
30. Amsler, C. D. (1996) Use of computer-assisted motion analysis for quantitative measurements of swimming behavior in petrichously flagellated bacteria, *Anal. Biochem. 235*, 20–25.
31. Sager, B. M., Sekelsky, J. J., Matsumura, P., and Adler, J. (1988) Use of a computer to assay motility in bacteria, *Anal. Biochem. 173*, 271–277.
32. Kondoh, H., Ball, C. B., and Adler, J. (1979) Identification of a methyl-accepting chemotaxis protein for the ribose and galactose chemoreceptors of *Escherichia coli*, *Proc. Natl. Acad. Sci. U.S.A. 76*, 260–264.
33. Newcomer, M. E., Lewis, B. A., and Quiocho, F. A. (1981) The radius of gyration of L-arabinose-binding protein decreases upon binding of ligand, *J. Biol. Chem. 256*, 3218–3222.
34. Feigin, L. A., and Svergun, D. I. (1987) *Structure Analysis by Small Angle X-ray and Neutron Scattering*, Plenum Press, New York.
35. Guinier, A., and Fournet, G. (1955) *Small Angle Scattering of X-rays*, John Wiley & Sons Inc., New York.
36. Borrok, M. J., Kiessling, L. L., and Forest, K. T. (2007) Conformational changes of glucose/galactose-binding protein illuminated by open, unliganded and ultra-high-resolution ligand-bound structures, *Protein Sci. 16*, 1032–1041.
37. Zhang, Y. H., Mannering, D. E., Davidson, A. L., Yao, N. H., and Manson, M. D. (1996) Maltose-binding protein containing an interdomain disulfide bridge confers a dominant-negative phenotype for transport and chemotaxis, *J. Biol. Chem. 271*, 17881–17889.
38. Li, M. Y., Ni, N. T., Chou, H. T., Lu, C. D., Tai, P. C., and Wang, B. H. (2008) Structure-based discovery and experimental verification of novel Al-2 quorum sensing inhibitors against *Vibrio harveyi*, *ChemMedChem 3*, 1242–1249.
39. Neiditch, M. B., Federle, M. J., Miller, S. T., Bassler, B. L., and Hughson, F. M. (2005) Regulation of LuxPQ receptor activity by the quorum-sensing signal autoinducer-2, *Mol. Cell 18*, 507–518.
40. Cheng, Y., and Prusoff, W. H. (1973) Relationship between inhibition constant (K_i) and concentration of inhibitor which causes 50% inhibition (I_{50}) of an enzymatic-reaction, *Biochem. Pharmacol. 22*, 3099–3108.
41. Fischetti, R., Stepanov, S., Rosenbaum, G., Barrea, R., Black, E., Gore, D., Heurich, R., Kondrashkina, E., Kropf, A. J., and Wang, S., *et al.* (2004) The BioCAT undulator beamline 18ID: a facility for biological non-crystalline diffraction and X-ray absorption spectroscopy at the Advanced Photon Source, *J. Synchrotron Radiat. 11*, 399–405.
42. Svergun, D., Barberato, C., and Koch, M. H. J. (1995) CRYSOL—A program to evaluate x-ray solution scattering of biological macromolecules from atomic coordinates, *J. Appl. Crystallogr. 28*, 768–773.
43. Brunger, A. T., Adams, P. D., Clore, G. M., DeLano, W. L., Gros, P., Grosse-Kunstleve, R. W., Jiang, J. S., Kuszewski, J., Nilges, M., and Pannu, N. S., *et al.* (1998) Crystallography & NMR system: a new software suite for macromolecular structure determination, *Acta Crystallogr., Sect D: Biol. Crystallogr. 54*, 905–921.
44. Murshudov, G. N., Vagin, A. A., and Dodson, E. J. (1997) Refinement of macromolecular structures by the maximum-likelihood method, *Acta Crystallogr., Sect D: Biol. Crystallogr. 53*, 240–255.
45. McRee, D. E. (1999) XtalView Xfit—A versatile program for manipulating atomic coordinates and electron density, *J. Struct. Biol. 125*, 156–165.
46. DeLano, W. L. (2002) *The PyMOL Molecular Graphics System*, DeLano Scientific, San Carlos, CA.
47. Takeo, K., Nakaji, T., and Shinmitsu, K. (1984) Synthesis of lycotetraose, *Carbohydr. Res. 133*, 275–287.